ADVANCED MATERIALS
www.advmat.de

Self-Stratifying Colored Radiative Cooling Paints Through Narrow-Band Color Preservation Scheme

*Dudong Feng, Andrew S. Witty, Fletcher I. Birnbaum, Orlando G. Rivera Gonzalez, Andrea Felicelli, Won-June Lee, Emily C. Barber, and Xiulin Ruan**

Although significant energy-saving potential of passive daytime radiative cooling has led to diffusively white or reflective surfaces, achieving coloration expands their application for both aesthetic and functional purposes. However, it presents huge technical challenges in scalable processing. This work presents a novel and general self-stratifying approach for creating radiative cooling paints with various colors using selected narrow-band absorption dyes. Applied as a single coat, these paints self-assemble into an absorption-scattering dual-layer structure that efficiently displays color while minimizing light absorption. Three base colors (cyan, magenta, and yellow) are demonstrated to provide full daytime subambient cooling, achieving 93% solar reflectance and 0.94 sky window emissivity. One newly developed black paint achieves 46.3% solar reflectance and a temperature drop of up to 25 °C, outperforming commercial counterparts. A purple radiative cooling paint (mixed dyes) demonstrates the color customization potential within the CMYK space, addressing the dilemma between color and cooling for colored radiative cooling paints. The mechanical and surface properties, characterized by abrasion, adhesion, and contact angle tests, are on par with or surpassing commercial products. This unique self-stratifying mechanism enhances surface properties and provides new insights for developing high-volume loading paints and water-harvesting coatings without increasing fabrication complexity.

1. Introduction

Energy consumption for thermal management in buildings, electronics, transportation, and human comfort represents a significant portion of daily energy use.[1,2] While conventional active cooling technologies, such as compression-evaporation cooling, are efficient and widely used, the use of environmentally harmful refrigerants and system components to control local temperatures leads to complex environmental impacts, including carbon emissions and ozone depletion, which contribute to global warming and climate change.[3] Passive cooling using natural cold reservoirs, such as water or wind, is often limited by location and the temperature difference between the reservoir and the cooling objects.[4–6] One vast cold resource we often overlook is the cold universe (3 K), providing ≈100 W m^{-2} of cooling power ideally.[7] However, this energy source remains underutilized because the Earth's atmosphere only allows radiation in the 8–13 micron range to communicate with deep space.[8] Additionally, achieving daytime radiative cooling requires minimizing solar absorption. Therefore, a spectrally designed surface is necessary to effectively harness the cold energy from space while preventing interference from incident solar radiation.

Subambient daytime radiative cooling under direct sunlight has been achieved by various designs,[9–13] including paints,[7,14–16] nanocomposite films,[17,18] photonic structural configurations,[19–21] polymer-on-metal multilayered structures,[22,23] and bio-inspired configurations.[24,25] To achieve a record high solar reflectance and higher cooling performance, daytime radiative cooling designs yield to be mirror-like or diffusive white surfaces. However, while the weather and location of daytime radiative cooling applications vary, higher radiative cooling performance does not necessarily lead to greater annual energy saving for buildings due to heating penalty.[26] For aesthetic purposes and diverse application scenarios, offering colored radiative cooling (CRC) designs would provide mutually beneficial solutions, enhancing both functionality and utility.

From the perspective of thermal radiation, coloration on surfaces leads to heating for daytime radiative cooling, since passive color appearance on opaque surface corresponds to visible light absorption. The color appearance and radiative cooling performance of CRC are mutually contradictory under passive condition.[27,28] Facing with this dilemma, searching for efficient color preservation solutions for daytime CRC becomes critically important. Structural color achieved by complex photonic

D. Feng, A. S. Witty, F. I. Birnbaum, O. G. R. Gonzalez, A. Felicelli, E. C. Barber, X. Ruan
School of Mechanical Engineering and the Birck Nanotechnology Center
Purdue University
West Lafayette, IN 47907, USA
E-mail: ruan@purdue.edu

W.-J. Lee
James Tarpo Jr. and Magaret Tarpo Department of Chemistry
Purdue University
West Lafayette, IN 47907, USA

The ORCID identification number(s) for the author(s) of this article can be found under https://doi.org/10.1002/adma.202504382

[Correction added on September 3, 2025, after first online publication: Affiliation of W.-J.L. has been corrected.]

DOI: 10.1002/adma.202504382

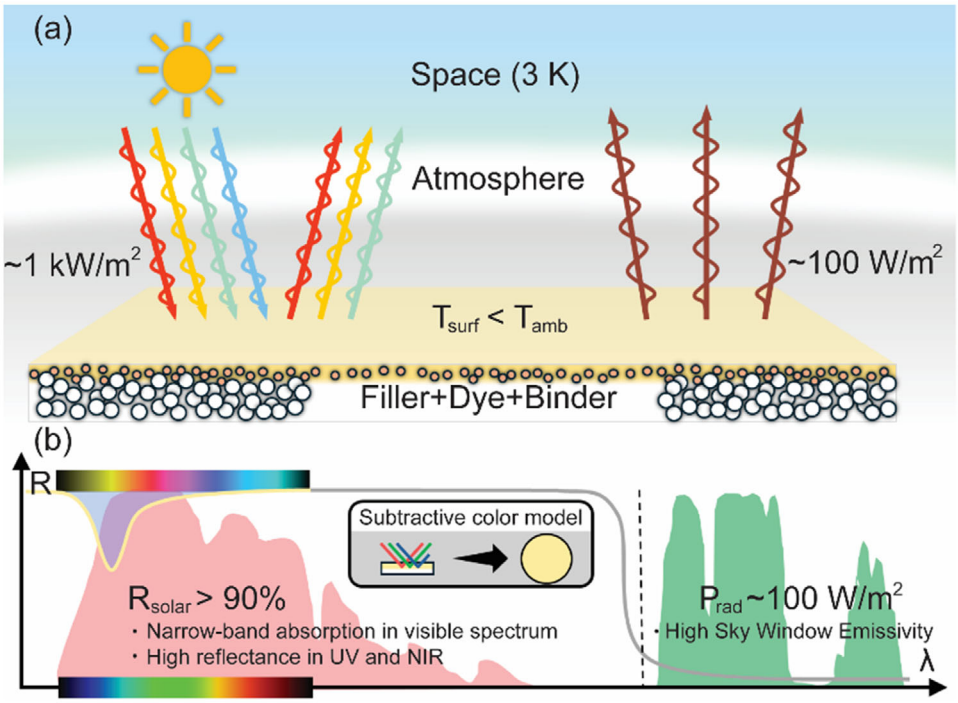

Figure 1. a) The mechanism of radiative cooling paint with dual layer structure. b) The mechanism of CRC paint and subtractive color model.

structures can achieve narrow-band absorption in visible range.[29–33] However, both multilayered (1D) and surface (2D) photonic structures require specialized cleanroom fabrication process and are expensive to scale up. Another common approach to achieving daytime CRC materials with good scalability is using organic or inorganic colorants (with or without fluorescent effect) to create a colored nanocomposite coating with narrow-band absorption features.[34] However, most radiative cooling nanocomposite coatings require both multilayered structures and precise thickness control of the colored layers,[35–41] which increases fabrication complexity and reduces the robustness of the material. Inorganic pigments are typically semiconductor materials, where light with energy greater than the bandgap is absorbed, leading to excessive solar absorption. Only materials with a large bandgap, such as Bi_2O_3,[42] are potential candidates for colored pigments. These materials are typically yellow because they absorb ultraviolet (UV) light (5–7% of total solar radiation) and visible light near the UV spectrum, making them potentially capable of achieving daytime CRC. Although such materials are UV-stable and exhibit excellent chemical durability, implementing a comprehensive color preservation scheme using inorganic dyes or pigments would be highly challenging.

In this work, we present a self-stratifying paint solution that achieves various colors in the CMYK (Cyan, Magenta, Yellow, and Key, which means Black) subtractive color space while maintaining radiative cooling functionality. Benefiting from four carefully selected narrow-band absorption dyes and a systematically tuned recipe through multiple iterations, these paints feature three-layer structure of acrylic, $BaSO_4$-acrylic, and $BaSO_4$-air (from here on, referred as acrylic/$BaSO_4$-acrylic/$BaSO_4$-air), that efficiently displays color while maintaining strong radiative cooling performance. We achieve over 90% solar reflectance for CMY (Cyan, Magenta, and Yellow) colors and 44% for black color with an acrylic-based self-layered paint. Additionally, we used a water-based binder to further improve the solar reflectance of a black radiative cooling paint, which can reach above 46%. Leveraging this stratified structure, the top layer made of pure binder serves as a protective coating, enhancing the surface properties of CRC paints. The low contact angle hysteresis indicates the potential for self-cleaning capabilities. Both acrylic based and water-based recipes demonstrate adhesion strength as commercial paints on glass slides and exhibits low mass loss in abrasion tests. This density-induced self-stratifying process automatically forms multilayered, multi-functional coatings in a single application step, significantly simplifying the process and expanding its potential applications. This new color preservation scheme offers a systematic solution for color customization in the CRC paint industry, making radiative cooling paint more promising and widely applicable in daily life.

2. Results and Discussion

2.1. Mechanism of Colored Radiative Cooling Paint

Subambient CRC can be achieved through high solar reflectance and high emissivity at the sky window. As shown in **Figure 1a**, the peak solar irradiation on a sunny day can reach 1 kW m^{-2}, while the typical maximum emissive power at the sky window is ≈100 W m^{-2}.[6] Based on the first law of thermodynamics and assuming no additional heat input from the environment, the temperature of a colored surface can remain below ambient throughout the day if the solar reflectance exceeds 90%.[7] In other words, we must efficiently use the 10% solar absorption to create as much color as possible without compromising the subambient

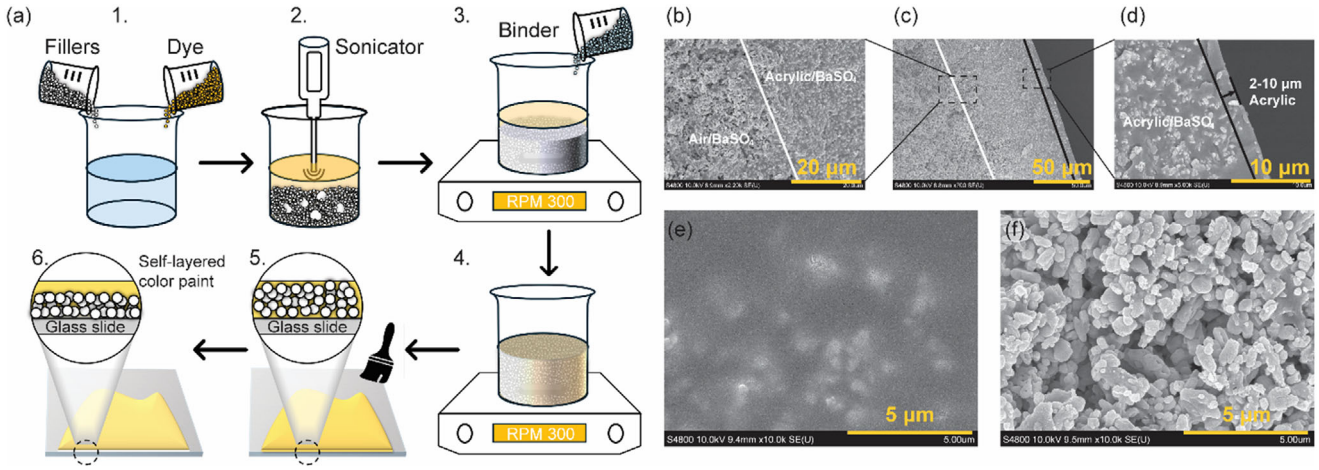

Figure 2. a) The fabrication process of a self-stratifying CRC paint. SEM images of the cross section at different magnification scales b–d), the top surface e), and bottom surface f) of a self-stratifying CRC paint.

radiative cooling function. One common coloration strategy for nanocomposite materials is to create an absorption-scattering dual-layer structure (shown in Figure 1a). Instead of searching for colored pigments with visible narrow-band absorption and strong near-infrared (NIR) scattering properties, we chose to use narrow-band absorption dyes to create a top colored layer, along with a strong scattering filler to reflect back the remaining light outside the visible spectrum. Both the top and bottom layer thicknesses need to be carefully designed. The top layer thickness should be controlled to avoid unnecessary absorption that does not contribute to coloration, while the bottom layer should be thick enough to scatter as much light as possible without allowing excessive transmission. Visible narrow-band dyes with <100 nm FWHM (full width at half maximum) and different peak wavelengths are necessary to create more vivid colors without excessively increasing solar energy absorption. Instead of using the conventional additive coloration model to describe the color, the subtractive color model, such as CMYK, would be more thermodynamically suitable for color customization in radiative cooling paint. As shown in Figure 1b, a yellow surface can be created by absorbing blue-color wavelengths, which is the complementary color to yellow in the complementary color spectrum. Color mixing can still be achieved by combining the four base colors, but within the subtractive color space.

As mentioned earlier, current CRC coatings require a multistep deposition process, which reduces the simplicity of application and the durability of the product. Here, we present a self-stratifying paint recipe that can produce functionally graded materials in a single step. As shown in **Figure 2**a, we first mix $BaSO_4$ filler and dye with isopropyl alcohol (IPA). Then, we use an ultrasonicator to break up the small filler clumps, with parafilm covering the top to prevent the evaporation of IPA. After that, we slowly pour in acrylic while stirring at 300 rpm. The stirring speed is critical for CRC paint compared to ultrawhite paint. High stirring speeds can introduce more air bubbles into the paint, which help with light scattering but disrupt the stratified structure and surface finish. For CRC, however, a multilayered structure and good surface finish are essential, so it is necessary to keep the stirring speed below 300 rpm. After stirring for 12–24 h, the paint is applied to a glass slide, where it automatically forms an absorption-scattering dual-layer structure after 24 h curing process (fabrication details in the Methodology and Experimental Section). This production recipe covers large sectors of applications, including flat roofs and low-slope roofs. In addition, roof coatings can be fabricated with our approach on flat lines in factories and later installed on roofs with any slopes.

SEM images of the cross-section of this self-stratifying paint (cyan) are shown in Figure 2b–d. As a result, the paint settles into an acrylic-$BaSO_4$/acrylic-$BaSO_4$/air structure. The concentration of acrylic decreases from top to bottom, while the concentration of $BaSO_4$ follows the reverse pattern. The complete opposite distribution preference can be explained by the phase separation of binder and filler, which is common when the volume loading of $BaSO_4$ reaches 58%. We found that formulations between 55% and 60% offered the most consistent, crack-free coatings upon drying. This aligns with our previous work, which identified ≈60% particle volume concentration as optimal for ultrawhite cooling paints,[7,14,15,43,44] to balance optical and mechanical properties. The main driving force behind this phenomenon could be a combination of two factors: the significant density difference between $BaSO_4$ (4.5 g cm^{-3}) and acrylic (1.18 g cm^{-3}), and the preference of polar particles toward the glass slide.[45,46] The top dyed acrylic layer, typically 2–10 μm thick, serves as the absorption layer to create the desired color, while the middle $BaSO_4$/acrylic layer (50-100 μm) and the bottom $BaSO_4$/air layer function as the scattering layers. Additionally, the top acrylic layer not only serves as the colored surface but also exhibits excellent mechanical and surface properties, which will be discussed later. Figure 2e shows a completely featureless view of the top surface ($BaSO_4$ particles covered by acrylic layer), indicating a very smooth surface finish. Those white spots represent the $BaSO_4$ particles buried beneath the acrylic as the top acrylic layer is not uniform thick. Figure 2f displays the bottom surface of the paint in contact with the glass slide. To clarify, the bottom layer is not purely $BaSO_4$ and air. As seen in Figure 2f, there are still some $BaSO_4$ particles encased in the acrylic. Note that these SEM images were taken from cyan radiative cooling paint. All other acrylic-based CRC paints possess similar structures, including

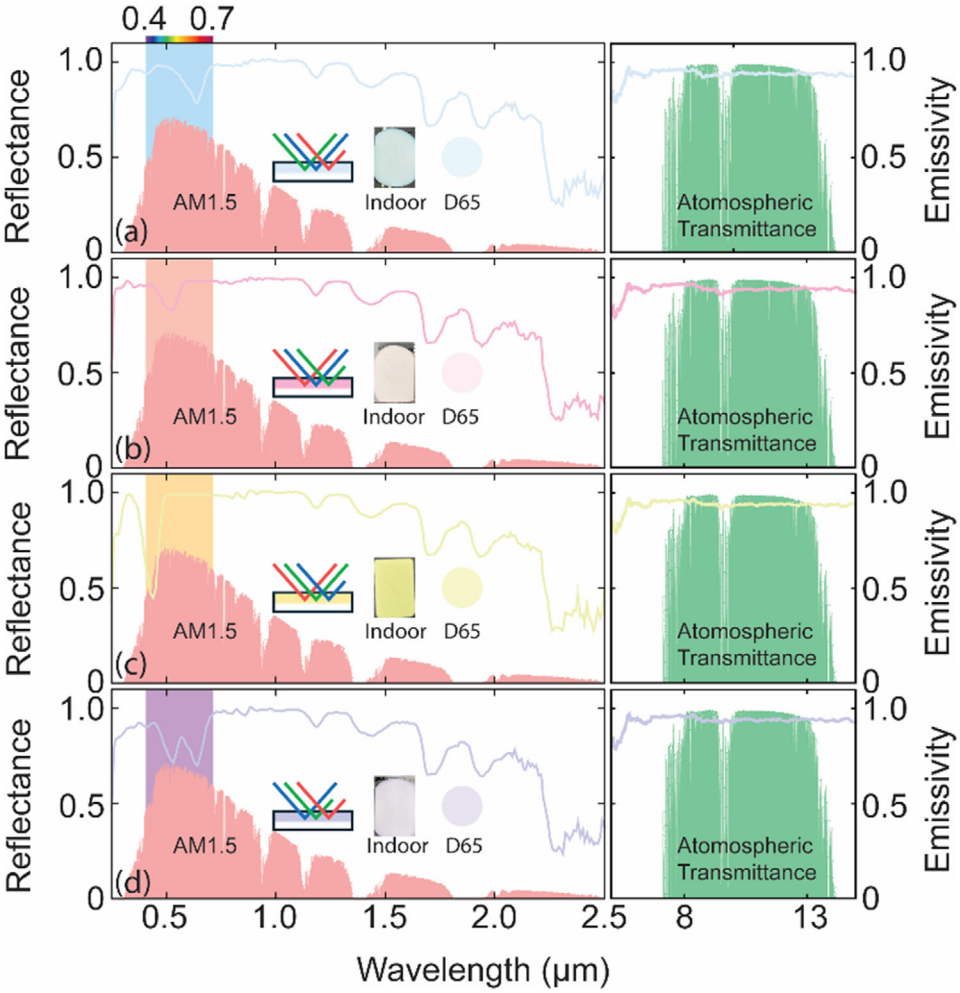

Figure 3. The spectral hemispherical solar reflectance and sky window emissivity of a) cyan, b) magenta, c) yellow, and d) purple radiative cooling paints. The real sample under indoor light conditions is presented in the inserted rectangular figure for each color, while the circular dots represent calculated values for CRC paints based on spectral reflectance under the D65 condition (noon solar light). Note that all samples are optically thick with less than 1% solar transmittance (shown in Figure S2, Supporting Information).

the silicone-based black radiative cooling paint (see Figure S1 in Supporting Information).

2.2. Performance of the Colored CRC Paints

The diffusive optical response in the solar spectrum (0.25–2.5 μm) and sky window range are characterized by optical spectroscopies with an integrating sphere, respectively (details in the Experimental Section). As shown in **Figure 3**a–c, the cyan, magenta, and yellow radiative cooling paints all exhibit narrow-band absorption within the visible range from 0.4–0.7 μm[47,48] (shaded area) and maintain very high reflectance in the UV (0.25–0.4 μm) and NIR range (0.7–2.5 μm). As explained in the previous section, based on the subtractive color model, the cyan color on the paint appears because the top layer absorbs part of its complementary color, red, and reflects the rest of the light. The same mechanism applies to magenta and yellow. **Table 1** summarizes the optical metrics of these three base color paints. All of them exhibit over 90% solar reflectance and around 1% solar transmission, ensuring that most of the solar energy is reflected back. The visible reflectance is 91.8% for cyan, 93.2% for magenta, and 89.6% for yellow, which are all lower than the total solar reflectance. This

Table 1. The reflectance and transmittance of four different CRC paints at solar spectrum (0.25–2.5 μm), visible spectrum (0.4–0.7 μm), UV spectrum (0.25–0.4 μm), and NIR (0.7–2.5 μm), as well as the emissivity of atmospheric window (7–15 μm).

	Cyan	Magenta	Yellow	Purple
R_{solar}	93.3%	93.3%	92.2%	88.7%
T_{solar}	0.6%	1.3%	0.9%	0.7%
R_{vis}	91.8%	93.2%	89.6%	82.6%
R_{UV}	95.3%	95.9%	87.9%	91.9%
R_{NIR}	94.4%	93.4%	94.3%	93.3%
ϵ_{sw}	0.942	0.943	0.942	0.942

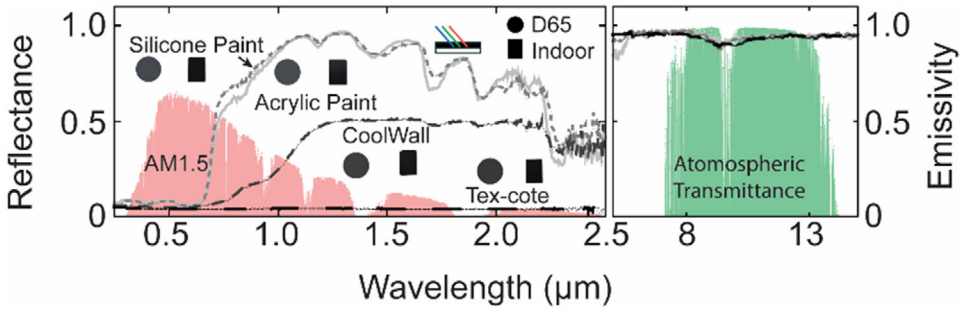

Figure 4. The spectral hemispherical solar reflectance and sky window emissivity of acrylic-based paint, silicone-based paint, and two commercial paints from Tex-Cote. The CoolWall paint is claimed to have better cooling performance than conventional black paint. The rectangular photos show real samples taken under indoor light conditions, while the circular dots represent calculated values for black paints based on spectral reflectance under the D65 condition (noon solar light). Note that all samples are optically thick with less than 1% solar transmittance (shown in Figure S2, Supporting Information).

indicates that narrow-band absorption is efficient, and solar absorption is utilized to create color within the visible range. Maintaining high NIR reflectance is crucial for achieving high solar reflectance, as NIR contributes more than 50% of the total solar spectrum. All three colors show 93–94% NIR reflectance, indicating that the top dyed layer is highly transparent to NIR light. We also calculated the reflectance in the UV range, as there is ≈60–70 W m^{-2} of peak solar energy in the UV range. Except for the yellow paint, cyan and magenta paints maintain 95% UV reflectance. The yellow paint shows 88% UV reflectance due to the tail effect of the narrow-band absorption. The right part of each figure in Figure 3 indicates that all three radiative cooling paints exhibit a high sky window emissivity of 0.94, as shown in Table 1. Additionally, to demonstrate the addition of dye in the subtractive color model, we present the purple color, which incorporates double narrow-band absorption while maintaining the same high sky window emissivity (shown in Figure 3d). These two narrow-band absorptions correspond to those in cyan and magenta. Since equal amounts of cyan and magenta dyes are used, the solar reflectance of the purple paint is only 88%, which may not fully achieve subambient radiative cooling on high solar irradiation days. However, by adjusting the dye amounts of the three CMY colors, we provide a potential efficient coloration scheme for radiative cooling paint that offers either subambient cooling or simply cooler performance compared to conventional paints. Investigation on dye selection could simultaneously achieve a more saturated color appearance and improved radiative cooling performance.

According to the subtractive color model, CMY dyes can theoretically create black by mixing all three base colors. However, in reality, black dye is necessary to achieve a true black color, rather than just a composite black.[49] Therefore, searching for effective black dyes for radiative cooling purposes is essential to complete this color preservation scheme based on the CMYK model. The definition of black color is 100% absorption of incoming visible light.[47] It is very unlikely to achieve subambient black radiative cooling paint, as visible light constitutes nearly 42% of total solar energy, which greatly exceeds the maximum sky window emissive power. The primary goal for black radiative cooling paint is to reflect as much NIR and UV as possible while maintaining its black color.

Table 2. The reflectance and transmittance of four different black radiative cooling paints at solar spectrum, visible spectrum, UV spectrum, and NIR, as well as the emissivity of atmospheric window, color-preserved reflecting power, and lightness value in Munsell color system.

	Acrylic paint	Silicone paint	CoolWall	Tex-Cote
R_{solar}	44.5%	46.3%	17.8%	4.0%
T_{solar}	0.2%	0.4%	0.0%	0.0%
R_{vis}	8.7%	8.5%	5.1%	4.0%
R_{UV}	7.9%	7.3%	5.2%	4.2%
R_{NIR}	74.5%	78.0%	28.4%	4.1%
ϵ_{sw}	0.943	0.944	0.938	0.935

Here, we developed both acrylic-based and silicone-based black radiative cooling paints, and both exhibit decent solar reflectance and sky window emissivity. As clearly shown in **Figure 4**, the acrylic-based and silicone-based black radiative cooling paints significantly outperform the two commercial products, CoolWall and Tex-Cote black paint in spectral solar reflectance, particularly in the NIR range. According to the performance metrics in **Table 2**, the acrylic-based paint achieves 44.5% total solar reflectance with a 75% NIR reflectance, while the silicone-based paint exceeds 46% solar reflectance with 78% NIR reflectance. The visible reflectance of the silicone-based paint is 8.5%, which is higher than that of the acrylic-based paint, indicating that the silicone-based paint appears potentially blacker than the acrylic-based paint. This slightly outperforming in solar reflectance of silicone-based paint is due to silicone's lower absorption in the NIR compared to acrylic. Despite claims that CoolWall is specially designed as a cool black paint, it shows only 18% solar reflectance due to its NIR reflectance of ≈28%, while Tex-Cote black paint, a conventional black paint, exhibits a low 4% solar reflectance. The right side of Figure 4 shows that all four paints have high spectral emissivity in the sky window, with a total value around 0.94 (Table 2).

We have demonstrated the solid solar reflectance of two newly developed black paints compared to commercial products. However, one might argue that our high solar reflectance partially stems from the high visible reflectance, suggesting that the black

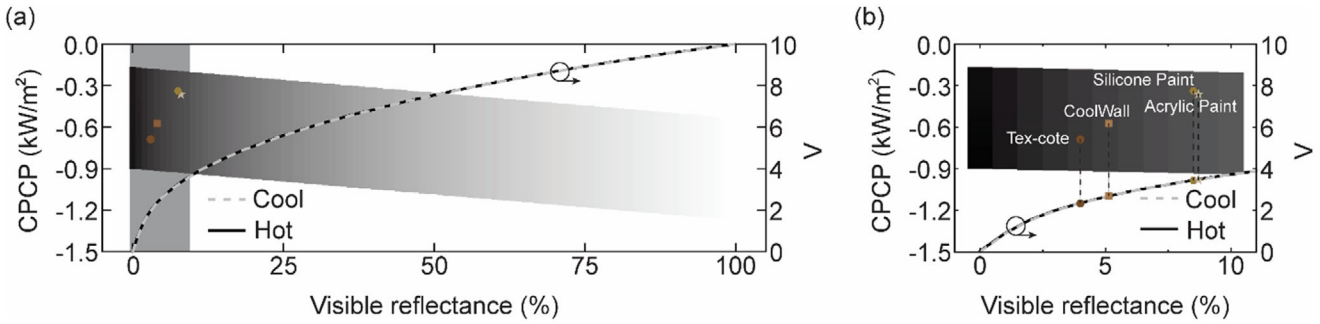

Figure 5. The color-preserved cooling power and lightness values (V) in the Munsell color model, with respect to visible reflectance (R_{vis}) on a a) 0–100% scale and b) 0–10% scale.

color is not pure enough. Therefore, to create a fair measure of a black radiative cooling surface, we propose a new indicator called color-preserved cooling power (CPCP), which is defined as follows:

$$CPCP = RP_{UV} + RP_{NIR} - RP_{vis} + E_{MIR} - I_{solar} \quad (1)$$

where the reflective power for different wavelength range (UV, visible, and NIR) can be calculated using $RP = \int r(\lambda) I_{\mathrm{AM1.5}}(\lambda) d\lambda$, the emissive power at sky window/mid-infrared (MIR) is given as $E_{MIR} = \int_{MIR} \epsilon_{atm}(\lambda) I_{\mathrm{BB}}(T_e, \lambda) d\lambda$, and the peak solar irradiation can be calculated by $I_{solar} = \int_{solar} I_{\mathrm{AM1.5}}(\lambda) d\lambda$. where λ is the wavelength, r is the spectral solar reflectance and ϵ_{atm} is the emissivity of the sky window. $I_{\mathrm{AM1.5}}$ is the AM1.5 solar intensity spectrum, and I_{BB} is the spectral blackbody radiation intensity at a specific temperature ($T_e = 300$ K). Compared to the standard cooling power used by the community, here in CPCP the RP_{vis} term becomes a penalty instead of a gain because it degrades the black color. Given a fixed visible reflectance, there are various UV and NIR reflectance that could exhibit a wide range of CPCP. The upper limit of the CPCP, representing the coolest UV and NIR spectrum at this visible reflectance, occurs when $R_{UV} = R_{NIR} = 100\%$, while the lower limit of the CPCP, representing the hottest UV and NIR spectrum at this visible reflectance, occurs when $R_{UV} = R_{NIR} = 0$. With these two bounds, we generate a gradient diamond grayscale map to reflect the blackness on the Cartesian coordinate of CPCP and visible reflectance, as shown in **Figure** 5a. To numerically illustrate the blackness of the color appearance, the lightness value (V) is calculated from the Munsell color system,[50] which provides a more perceptually uniform color space from black to white compared to other color spaces.[51] We also calculate the corresponding color to align with the coolest and hottest conditions at the same visible reflectance. The gray dashed line and the solid black line overlap, indicating that the color difference between the coolest and hottest color is not noticeable. This suggests that including a larger visible spectrum range (e.g., 360–830 nm) is unnecessary, as the stimuli of light outside the 400–700 nm range on the human eye is negligibly low. With this R_{vis}-CPCP blackness map, the cooling performance of colors with different V values can be compared. For instance, as shown in Figure 5b, the acrylic paint has a lightness value of 3.1 with a CPCP of -352.5 W m^{-2}, while the silicone paint has a lightness value of 3 with a higher CPCP of -335.0 W m^{-2}. This indicates that the silicone paint maintains a blacker appearance while offering better potential cooling power, i.e., less heating because both cooling powers are negative. However, in the case of CoolWall or Tex-cote, drawing a similar conclusion is challenging. Although our two black paints exhibit much better CPCP than CoolWall (-565.7 W m^{-2}) and Tex-Cote (−680.9 W m^{-2}), both CoolWall and Tex-Cote appear blacker than our two black paints. Therefore, no meaningful conclusion can be made by these comparisons, as it is challenging to evaluate how much cooling power should compensate for the reduction in blackness. To develop a practical evaluation for black radiative cooling paint, if the difference in V value is less than 1, the color difference is generally considered a Just Noticeable Difference (JND) to the human eye. The V value of CoolWall and Tex-cote are 2.6 and 2.3, respectively. Based on this criterion, the four black paints can be categorized as having a similar blackness. In this context, we can conclude that our paints exhibit better cooling performance compared to benchmark products, which include both commercial black radiative cooling paint and conventional black paint. However, the JND criteria in V value is negotiable and can vary depending on the specific requirements of real-world applications. Note that the hue and chroma in the Munsell color system remain constant (with no variation in spectral visible reflectance), as we assume these two curves represent colors along the greyscale bar, where neither hue nor chroma changes. Both the V values of the acrylic-based and silicone-based paints fall outside the bounds of the two curves, indicating that these two black colors are slightly deviating from the pure greyscale bar.

To illustrate the improvement of this newly proposed index, we would refer to the definition of conventional cooling power of a radiative cooling surface, which can be calculated based on energy balance:

$$CP = RP_{UV} + RP_{NIR} + RP_{vis} + E_{MIR} - I_{solar} \quad (2)$$

We also plot the conventional cooling power-R_{vis} map in Figure S3 (Supporting Information). The difference between Figure 5a and Figure S3a (Supporting Information), or Figure 5b and Figure S3b (Supporting Information), is caused by the sign before the visible reflective power, which is clearly shown by comparing Equations (1) and (2). By doing so, the darkest color

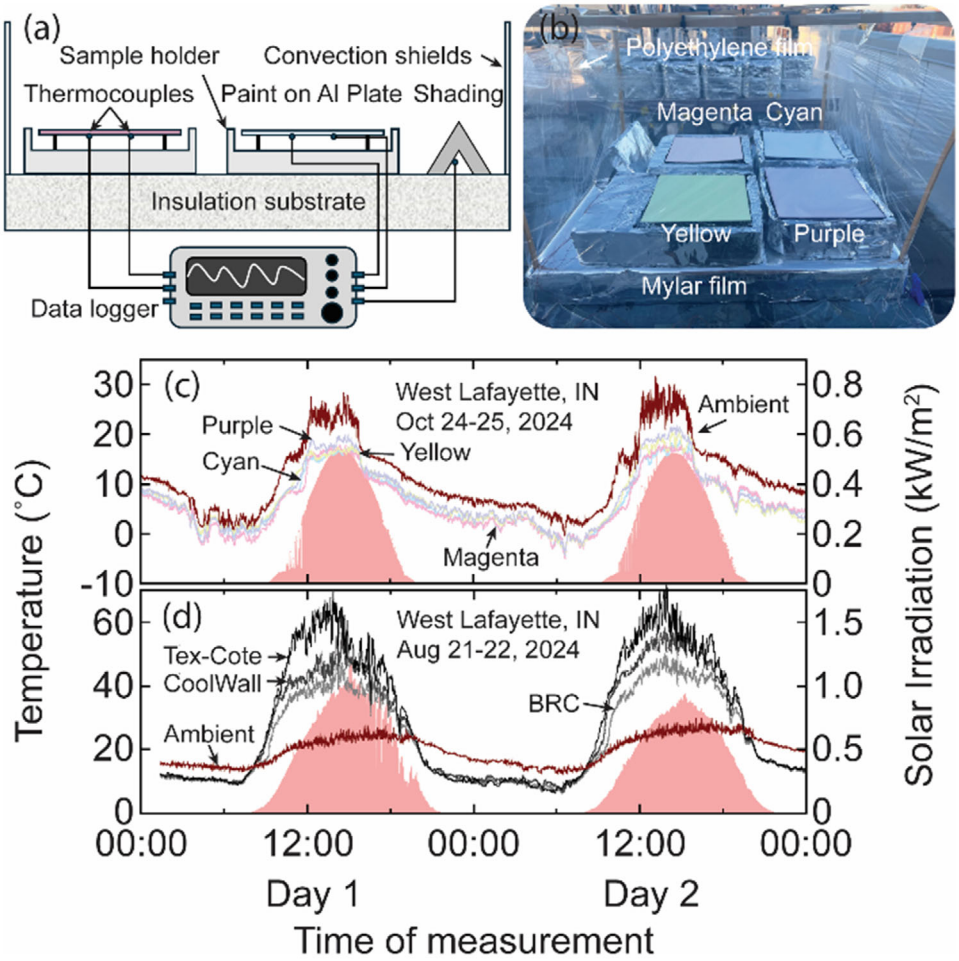

Figure 6. a) The schematic and b) photograph of the field test setup for temperature characterization. Temperatures of c) four colored and d) three black radiative cooling paints.

with the highest cooling power will exhibit the highest CPCP value. Physically speaking, the cooling power loss caused by color preservation is not considered a penalty but rather a credit. When combined with the V value in the Munsell color space model, CPCP can be used to directly evaluate the radiative cooling potential of two close colors (with less than JND), providing a more comprehensive understanding of their performance.

Onsite field tests were performed for all radiative cooling paints and commercial black paints. The setup is shown in **Figure** 6a,b. Paint samples were applied to a thin aluminum plate (6 in × 6 in, 1 mm thick), with thermocouples (Omega T type) placed beneath the plate to measure temperature. The samples were elevated using wooden posts to minimize heat conduction from the bottom, and the sample holder was wrapped in Mylar film (a high solar reflectance film) to reduce solar absorption by the surrounding environment, which could affect the local temperature during measurement. The chamber was also wrapped with convection shields made of polyethylene film to prevent the effects of convection. Environmental heat leakage from convection and conduction has been suppressed and controlled to ≈1 W. The chamber temperature was monitored using a shaded thermocouple to eliminate local heating effects. All thermocouple data was recorded by a data logger (Graphtec Midi Logger GL840), and the solar irradiance was measured using the weathering station (Ambient Weather WS-2000 Smart Weather Station). The wind speed and humidity data are presented in Figure S4 (Supporting Information).

As shown in Figure 6c, all four CRC paints achieved full subambient daytime cooling with solar irradiation around 500 W m^{-2} on October 24–25, 2024, in West Lafayette, IN. During nighttime, the CRC paints provided a temperature drop of 1–3 °C below ambient, while during the daytime, they maintained a temperature of ≈4–15 °C below ambient. Around 1 PM, the maximum temperature drops below ambient reached up to 15 °C. The purple radiative cooling paint performed slightly lower than the other three, as it has lower solar reflectance. However, it still achieved full subambient daytime cooling (24 h), which can be attributed to the relatively low solar irradiance during the fall season. The field test results for the black radiative cooling paints are shown in Figure 6d. None of the three black paints were able to achieve subambient daytime radiative cooling. However, the newly developed black paint outperformed CoolWall paint by 10 °C and the commercial black paint by 25 °C during peak solar irradiation. Since the acrylic-based paint shares very similar

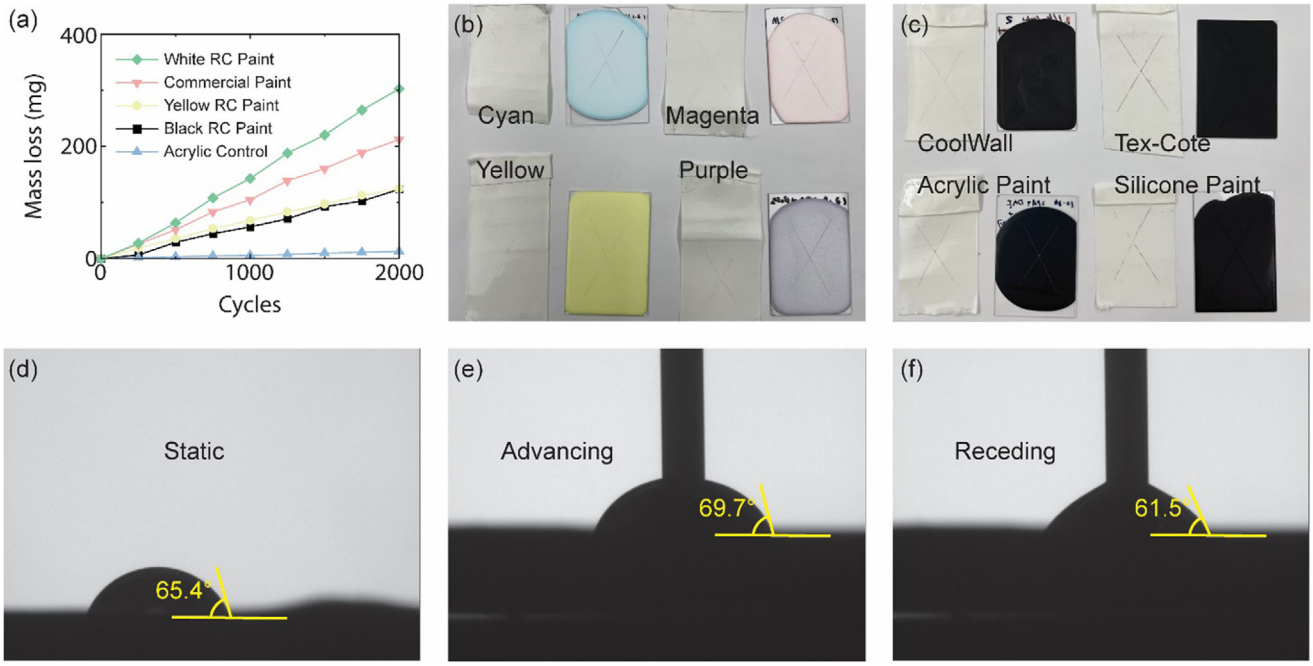

Figure 7. a) Abrasion test on the ultrawhite $BaSO_4$ paint,[14] commercial paint, yellow radiative cooling paint, black silicone-based paint, and pure acrylic film as a control reference according to ASTM D4060.[52] Adhesion test on b) four CRC paints and c) black radiative cooling and commercial paints according to ASTM D3359-23.[53] The static d), advancing e), and receding f) contact angle of cyan paint.

properties with the silicone-based paint, field testing was not performed for simplicity. Overall, the two black radiative cooling paints offer significant energy savings compared to both conventional black paint and commercial cool black paint.

2.3. Mechanical and Surface Properties of CRC Paints

To demonstrate the advantages of this self-stratifying multilayered structure, we performed abrasion tests on CRC paints compared to ultrawhite $BaSO_4$ paint,[14] commercial paints, and pure acrylic film as a control reference. The surface mechanical properties were characterized by mass loss using the Taber Abraser. The weight of samples was measured after every 250 cycles, with a refacing process every 500 cycles. As shown in **Figure** 7a, with the protective effect of the top binder layers in the acrylic and silicone paints, the mass losses of these two paints are more than that of the acrylic film, but significantly lower than that of the commercial and ultrawhite $BaSO_4$ paints. Notably, the volume loading of these CRC paints is the same as that of the ultrawhite $BaSO_4$ paint with a high volume fraction of 60%. This self-stratifying paint recipe ensures robust surface mechanical strength for high-volume loading CRC paints without increasing fabrication complexity.

Additionally, adhesion tests were performed based on the X-cut tape test. The detailed characterization process can be found in ref. [53]. Based on the residual paint on the test tape, all CRC paints were classified as 4A (less than 5% loss), the same as the two commercial black paints (shown in Figure 7b,c). Adhesion tests were conducted after 250 h of weathering exposure (ISO 11 341 Cycle A, Method 1). Shown in Figure S5 (Supporting Information), most CRC and black radiative cooling paints maintained a 4A adhesion level, whereas purple and cyan coatings dropped to 2A and 3A, respectively. The reduced adhesion is likely due to the high-volume loading of $BaSO_4$, which can weaken binder–substrate interactions over prolonged exposure. As shown by the SEM images earlier, the CRC paints have a smooth surface finish. The contact angles were measured to characterize the surface properties of this multilayered structure. As shown in Figure 7c, the static contact angle of these CRC paints is 69.5°, indicating the surface hydrophilic. This is similar to the value for the acrylic film. However, the contact angle hysteresis (the difference between the advancing and receding contact angles, shown in Figure 7d,e, respectively) is relatively low at 8.2° (see Supporting Information for all remaining samples), which indicates that although water tends to stick to the surface, it can easily roll off with minimal activation energy. This property would be beneficial for atmospheric water harvesting and self-cleaning capabilities, particularly in inclined surface conditions.

3. Conclusion

In this work, we presented a new recipe for self-stratifying CRC paints with the potential to achieve all colors in the CMYK color space. This multilayered structure ensures an absorption-scattering design that efficiently displays color while maintaining high performance in daytime radiative cooling. With the assistance of carefully selected narrow-band dyes, all three CRC paints (CMY colors) achieved solar reflectance above 93% and sky window emissivity of 0.94. The purple radiative cooling paint created through dye mixing validates the dye mixing scheme, showing that it can be used to produce any color within the CMYK

color space. All four CRC acrylic-based paints achieved full daytime subambient cooling in field tests, with a maximum temperature drop of 15 °C below ambient. We also introduced two black self-stratifying radiative cooling paints using different binders, achieving record high solar reflectance up to 46.3% and almost 25 °C temperature drop below ambient. Abrasion, adhesion, and contact angle tests were performed to characterize the mechanical and surface properties of these CRC paints, which exhibited capabilities comparable to, and in some cases exceeding, those of commercial-level products. The self-stratifying structure demonstrates excellent abrasion resistance and strong adhesion capabilities, providing an easy-to-fabricate alternative for high-volume loading paints. The combination of hydrophilicity and low hysteresis makes this recipe a promising candidate for atmospheric water harvesting coatings, enhancing the versatility and effectiveness of radiative cooling technology in mitigating global warming.

4. Experimental Section

Optical Properties Calculations: The visible reflectance can be calculated as follows:

$$R_{vis} = \frac{\int_{vis} r(\lambda)\, I_{AM1.5}(\lambda)\, d\lambda}{\int_{vis} I_{AM1.5}(\lambda)\, d\lambda} \tag{3}$$

where λ is the wavelength, r is the spectral solar reflectance and $I_{AM1.5}$ is the AM1.5 solar intensity spectrum. The total reflectance at other spectrums (e.g., UV and NIR) can also be calculated by changing the integral range. The sky window emissivity is given by:

$$\epsilon_{sw} = \frac{\int_{MIR} \epsilon_{atm}(\lambda)\, I_{BB}(T_e, \lambda)\, d\lambda}{\int_{MIR} I_{BB}(T_e, \lambda)\, d\lambda} \tag{4}$$

where ϵ_{atm} is the emissivity of the sky window and I_{BB} is the spectral blackbody radiation intensity at a specific temperature.

Spectrum to Different Color Space: Human visual perceptions are an ability to perceive difference between light composed of different frequencies independently of light intensity with three kinds of cone cells (short, medium, and long).[47,51] To mathematically characterize the incoming light intensity, the Commission on Illumination (CIE) color space creates a "standard observer" that can map a range of physically produced color to tristimulus values, which is called XYZ color space. The mapping of the spectral reflectance of a real object under certain light condition to XYZ color space is through color matching functions as follows:

$$X = \frac{100 \int S(\lambda)\, r(\lambda)\, \bar{x}(\lambda)\, d\lambda}{\int S(\lambda)\, \bar{y}(\lambda)\, d\lambda} \tag{5}$$

$$Y = \frac{100 \int S(\lambda)\, r(\lambda)\, \bar{y}(\lambda)\, d\lambda}{\int S(\lambda)\, \bar{y}(\lambda)\, d\lambda} \tag{6}$$

$$Z = \frac{100 \int S(\lambda)\, r(\lambda)\, \bar{z}(\lambda)\, d\lambda}{\int S(\lambda)\, \bar{y}(\lambda)\, d\lambda} \tag{7}$$

where $\bar{x}$, $\bar{y}$, and $\bar{z}$ are the color matching function. $S(\lambda)$ is the D65 standard illumination (noon light). To map the XYZ value to a device color that can be reproduced on a display, the sRGB (standard RGB) color space is used. The conversion from XYZ to sRGB can be done using the following equations:

$$\begin{bmatrix} R \\ G \\ B \end{bmatrix} = \boldsymbol{M} \begin{bmatrix} X \\ Y \\ Z \end{bmatrix} \tag{8}$$

where $\boldsymbol{M}$ = [3.2404542, −1.5371385, −0.4985314; −0.9692660, 1.8760108, 0.0415560; 0.0556434, −0.2040259, 1.0572252]. After applying the matrix, the linear RGB values must be gamma-corrected to obtain non-linear RGB values:[54,55]

$$R = \begin{cases} 12.92R & if\ R \le 0.0031308 \\ 1.055R^{1/2.4} - 0.055 & otherwise \end{cases} \tag{9}$$

Note that this conversion should be performed for all three RGB values. The conversion from RGB to CMYK is given as follows:[56]

$$\begin{bmatrix} C \\ M \\ Y \end{bmatrix} = 1 - \begin{bmatrix} R \\ G \\ B \end{bmatrix} \tag{10}$$

and

$$K = \min(C, M, Y) \tag{11}$$

The Munsell color space was utilized to provide a more uniform evaluation of a color's blackness. Converting from XYZ to the Munsell color system was a non-trivial process because Munsell was based on human perception and is not mathematically derived from XYZ. Typically, the conversion was achieved using lookup tables or interpolation methods based on empirical data. However, several online tools and libraries in various programming languages were available to perform this conversion efficiently.[50]

Materials Selection and Fabrication Process: The fabrication process of the acrylic-based paint follows a series of detailed steps. Initially, the narrow-band dyes (Cyan: Epolight 5839, Magenta: Epolight 5396, Yellow: Epolight 5843) were diluted with N,N-Dimethylformamide (Millipore Sigma DX1730) at a concentration of 0.001 g mL^{-1}. 8 mL of 2-propanol (IPA) per gram of acrylic is added to a bottle. $BaSO_4$ (Sigma Aldrich 243353) was then slowly added to the IPA to achieve a final pigment volume concentration of 58%, the stir speed of a magnetic stirrer was fixed at 300 rpm for 15 min to ensure that the pigment particles are wetted and initially dispersed. The dye solution (or black dye powder: Epolight 7527A for black color) in DMF was then added, with the amount corresponding to the desired strength of the color (0.5 mL per gram of acrylic for Cyan, Magenta, and Yellow; 0.01 g per gram of acrylic for black dye). The mixture was sonicated for a total of 15 min, with intervals of 5 s on and 10 s off, at 10% amplitude using a Branson Digital Sonifier 250, with parafilm covering the bottle. The mixture is then stirred at 250–300 rpm, and acrylic powder (Elvacite 2028) is slowly added to prevent agglomeration. The final mixture is stirred for 16 h at 250–300 rpm. Finally, the paint was poured or brushed onto the desired substrate and left to cure for another 16 h.

The fabrication process of silicone-based paint was similar to that of the acrylic-based paint. Silikopur 8081 (Evonik) and deionized water were mixed at a weight ratio of 1:1.2 using a magnetic stir bar at 250 rpm for 15 min. $BaSO_4$ was then slowly added to achieve a final pigment volume concentration of 58%, followed by the addition of the colored dye solution or powder based on the desired color strength. The final mixture was stirred for a minimum of 4 h at 250–300 rpm to ensure complete particle dispersion while avoiding excessive bubble formation. Prior to application, the paint was degassed to remove any air bubbles formed during mixing. The paint was then left to cure through water evaporation for 16 h.

Based on our recent theoretical analysis of $BaSO_4$ thermal radiative properties, its dielectric function in both the visible range and the sky window range offers intrinsic advantages as a scattering center over other common fillers.[57] The particle size distributions were also examined for

both formulations in our recent studies,[14,43] which showed $BaSO_4$ particles had a hierarchical size distribution centered ≈400 nm. This hierarchical sizing strategy was validated through theoretical analysis.[58,59]

Optical Characterizations: The spectral reflectance and transmittance of all CRC paint samples (suspended samples) were measured from 250 nm to 2.5 µm using a Perkin Elmer Lambda 950 UV-Vis-NIR spectrometer with an integrating sphere setup. A certified Spectralon diffuse reflectance standard was used to characterize the measured raw data. The uncertainty of the solar reflectance was less than 1% based on the measurement of four samples. The spectral emissivity in the range of 2.5 to 20 µm was measured using a Nicolet iS50 FTIR with an integrating sphere from PIKE Technology. The estimated uncertainty in the measurements was 0.02, based on the mid-IR diffuse reflectance standard provided by PIKE Technologies. The UV, visible, NIR and total solar reflectance were calculated using Equation (3) and the sky window emissivity is calculated using Equation (4) shown in previous section.

Contact Angle Characterization: To characterize the wettability of the paint samples, the sessile drop test technique was performed with a 290 Ramé-Hart Goniometer. Both dynamic and static water contact angles were measured using deionized water. A 5 µL water droplet was dropped on the surface and the static angle is quick measured to avoid any gravitational effects on the contact angle measurements. For the measurement of the dynamic contact angle, a 5 µL water droplet was initially placed on the surface. The droplet volume was then gradually increased or decreased in increments of 0.25 µL using a micro-syringe. The advancing and receding contact angles were measured at the point where the boundary of the droplet began to move. The micro-syringe was positioned at the center of the droplet, close to the base contact line, to ensure even distribution of water addition and retraction.

Supporting Information

Supporting Information is available from the Wiley Online Library or from the author.

Acknowledgements

D.F. and A.S.W. contributed equally to this work. D.F. and X.L. acknowledge partial support from the US National Science Foundation through award 2102645. A.W. acknowledges the Cordier Fellowship from Purdue University, O.G.R.G., A.F., and E.B. each acknowledges a National Science Foundation Graduate Research Fellowship, E.B. acknowledges the Ingersoll-Rand Fellowship from Purdue University. W.-J.L. acknowledges the support from Ambilight Inc. under contract #4000187.02.

Conflict of Interest

The authors declare no conflict of interest.

Data Availability Statement

The data that support the findings of this study are available from the corresponding author upon reasonable request.

Keywords

color customization, cool black paint, colored radiative cooling paint, narrow-band absorption dyes, self-stratifying

Received: March 5, 2025
Revised: July 23, 2025
Published online: August 20, 2025

[1] H. Wang, Q. Chen, *Energy Build.* **2014**, *82*, 428.
[2] V. Munćan, I. Mujan, D. Macura, A. S. Anđelković, *Energy* **2024**, *304*, 132191.
[3] N. Abas, A. R. Kalair, N. Khan, A. Haider, Z. Saleem, M. S. Saleem, *Renewable Sustainable Energy Rev.* **2018**, *90*, 557.
[4] H. M. Daraghmeh, C.-C. Wang, *Appl. Therm. Eng.* **2017**, *114*, 1224.
[5] A. A. Alkrush, M. S. Salem, O. Abdelrehim, A. A. Hegazi, *International Journal of Refrigeration* **2024**, *160*, 246.
[6] J. Peoples, X. Ruan, in *Light, Plasmonics and Particles* (Eds.: M. P. Mengüç, M. Francoeur), Elsevier, AE Amsterdam, Netherlands **2023**, pp. 393–419.
[7] X. Li, J. Peoples, Z. Huang, Z. Zhao, J. Qiu, X. Ruan, *Cell Rep. Phys. Sci.* **2020**, *1*, 100221.
[8] A. W. Harrison, M. R. Walton, *Sol. Energy* **1978**, *20*, 185.
[9] B. Zhao, M. Hu, X. Ao, N. Chen, G. Pei, *Appl. Energy* **2019**, *236*, 489.
[10] S. Fan, W. Li, *Nat. Photonics* **2022**, *16*, 182.
[11] X. Yu, J. Chan, C. Chen, *Nano Energy* **2021**, *88*, 106259.
[12] X. Yin, R. Yang, G. Tan, S. Fan, *Science* **2020**, *370*, 786.
[13] Z. Li, Q. Chen, Y. Song, B. Zhu, J. Zhu, *Adv. Mater. Technol.* **2020**, *5*, 1901007.
[14] X. Li, J. Peoples, P. Yao, X. Ruan, *ACS Appl. Mater. Interfaces* **2021**, *13*, 21733.
[15] A. Felicelli, I. Katsamba, F. Barrios, Y. Zhang, Z. Guo, J. Peoples, G. Chiu, X. Ruan, *Cell Rep. Phys. Sci.* **2022**, *3*, 101058.
[16] P. Li, Y. Liu, X. Liu, A. Wang, W. Liu, N. Yi, Q. Kang, M. He, Z. Pei, J. Chen, P. Jiang, W. Li, H. Bao, X. Huang, *Adv. Funct. Mater.* **2024**, *34*, 2315658.
[17] Y. Zhai, Y. Ma, S. N. David, D. Zhao, R. Lou, G. Tan, R. Yang, X. Yin, *Science* **2017**, *355*, 1062.
[18] J. Mandal, Y. Fu, A. C. Overvig, M. Jia, K. Sun, N. N. Shi, H. Zhou, X. Xiao, N. Yu, Y. Yang, *Science* **2018**, *362*, 315.
[19] E. Rephaeli, A. Raman, S. Fan, *Nano Lett.* **2013**, *13*, 1457.
[20] A. P. Raman, M. A. Anoma, L. Zhu, E. Rephaeli, S. Fan, *Nature* **2014**, *515*, 540.
[21] M. M. Hossain, B. Jia, M. Gu, *Adv. Opt. Mater.* **2015**, *3*, 1047.
[22] L. Zhou, H. Song, J. Liang, M. Singer, M. Zhou, E. Stegenburgs, N. Zhang, C. Xu, T. Ng, Z. Yu, B. Ooi, Q. Gan, *Nat. Sustain.* **2019**, *2*, 718.
[23] P. Yang, C. Chen, Z. M. Zhang, *Sol. Energy* **2018**, *169*, 316.
[24] N. N. Shi, C.-C. Tsai, F. Camino, G. D. Bernard, N. Yu, R. Wehner, *Science* **2015**, *349*, 298.
[25] T. Li, Y. Zhai, S. He, W. Gan, Z. Wei, M. Heidarinejad, D. Dalgo, R. Mi, X. Zhao, J. Song, J. Dai, C. Chen, A. Aili, A. Vellore, A. Martini, R. Yang, J. Srebric, X. Yin, L. Hu, *Science* **2019**, *364*, 760.
[26] S. Wijesuriya, R. A. Kishore, M. V. A. Bianchi, C. Booten, *J. Cleaner Prod.* **2022**, *379*, 134763.
[27] B. Xie, Y. Liu, W. Xi, R. Hu, *Mater. Today Energy* **2023**, *34*, 101302.
[28] W. Xi, Y. Liu, W. Zhao, R. Hu, X. Luo, *Int. J. Therm. Sci.* **2021**, *170*, 107172.
[29] L. Zhu, A. Raman, S. Fan, *Appl. Phys. Lett.* **2013**, *103*, 223902.
[30] W. Li, Y. Shi, Z. Chen, S. Fan, *Nat. Commun.* **2018**, *9*, 4240.
[31] E. Blandre, R. A. Yalçin, K. Joulain, J. Drévillon, *Opt. Express* **2020**, *28*, 29703.
[32] T. Huang, Q. Chen, J. Huang, Y. Lu, H. Xu, M. Zhao, Y. Xu, W. Song, *ACS Appl. Mater. Interfaces* **2023**, *15*, 16277.
[33] G. J. Lee, Y. J. Kim, H. M. Kim, Y. J. Yoo, Y. M. Song, *Adv. Opt. Mater.* **2018**, *6*, 1800707.
[34] T. Yu, R. Liu, Z. Yang, S. Yang, Z. Ye, J. Lu, *Appl. Energy* **2025**, *377*, 124436.
[35] Y. Chen, J. Mandal, W. Li, A. Smith-Washington, C.-C. Tsai, W. Huang, S. Shrestha, N. Yu, R. P. S. Han, A. Cao, Y. Yang, *Sci. Adv.* **2020**, *6*, aaz5413.
[36] X. Wang, Q. Zhang, S. Wang, C. Jin, B. Zhu, Y. Su, X. Dong, J. Liang, Z. Lu, L. Zhou, W. Li, S. Zhu, J. Zhu, *Sci. Bull.* **2022**, *67*, 1874.

[37] S. Son, S. Jeon, D. Chae, S. Y. Lee, Y. Liu, H. Lim, S. J. Oh, H. Lee, *Nano Energy* **2021**, *79*, 105461.
[38] J. Xu, R. Wan, W. Xu, Z. Ma, X. Cheng, R. Yang, X. Yin, *Mater. Today Nano* **2022**, *19*, 100239.
[39] D. Chae, S. Y. Lee, H. Lim, S. Son, J. Ha, J. Park, J. H. Park, S. J. Oh, H. Lee, *ACS Appl. Mater. Interfaces* **2023**, *15*, 58274.
[40] T. Y. Yoon, S. Son, S. Min, D. Chae, H. Y. Woo, J.-Y. Chae, H. Lim, J. Shin, T. Paik, H. Lee, *Mater. Today Phys.* **2021**, *21*, 100510.
[41] H. Gonome, M. Baneshi, J. Okajima, A. Komiya, S. Maruyama, *J. Quant. Spectrosc. Radiat. Transfer* **2014**, *132*, 90.
[42] H. Zhai, D. Fan, Q. Li, *Sol. Energy Mater. Sol. Cells* **2022**, *245*, 111853.
[43] A. K. Aljwirah, X. Liu, O. Rivera Gonzalez, K. Alhammadi, W.-J. Lee, I. Katsamba, X. Ruan, *ACS Appl. Mater. Interfaces* **2025**, *17*, 32914.
[44] E. Barber, D. Feng, Z. Fang, D. Carne, O. R. Gonzalez, W.-J. Lee, N. Vansal, K. Raykova, X. Ruan, *ACS Appl. Opt. Mater.* **2025**, *3*, 1137.
[45] S. Zahedi, D. Zaarei, S. R. Ghaffarian, *J. Coat. Technol. Res.* **2018**, *15*, 1.
[46] I. Nikiforow, J. Adams, A. M. König, A. Langhoff, K. Pohl, A. Turshatov, D. Johannsmann, *Langmuir* **2010**, *26*, 13162.
[47] S. K. Shevell, *The Science of Color*, Elsevier Science, Kidlington, UK **2003**, pp. 149–190.
[48] F. P. Incropera, D. P. DeWitt, T. L. Bergman, A. S. Lavine, *Fundamentals of Heat and Mass Transfer*, Vol. *6*, Wiley, New York, **1996**.
[49] J. A. Siegel, *Forensic Chemistry: Fundamentals and Applications*, John Wiley & Sons, West Sussex, UK **2015**.
[50] P. Centore, *The Munsell and Kubelka-Munk Toolbox*, Available at: Munsell and Kubelka-Munk Toolbox (munsellcolourscienceforpainters.com) **2017**.
[51] M. D. Fairchild, *Color Appearance Models*, John Wiley & Sons, West Sussex, UK **2013**.
[52] A. International, *ASTM D4060-19: Standard Test Method for Abrasion Resistance of Organic Coatings by the Taber Abraser*, ASTM International, **2019**.
[53] A. International, *ASTM D3359-23: Standard Test Methods for Rating Adhesion by Tape Test*, ASTM International, **2023**.
[54] International Commission on, I., *Colorimetry*, 4th ed., CIE Central Bureau, Vienna, Austria, **2022**.
[55] C. International Electrotechnical, *IEC 61966-2-1:1999 (sRGB Standard) – Default RGB Colour Space – sRGB*, IEC, **1999**.
[56] H. R. Kang, *Color Technology for Electronic Imaging Devices*, SPIE press, Bellingham, Washington, USA **1997**.
[57] Z. Tong, J. Peoples, X. Li, X. Yang, H. Bao, X. Ruan, *Mater. Today Phys.* **2022**, *24*, 100658.
[58] D. Carne, J. Peoples, F. Arentz, X. Ruan, *Int. J. Heat Mass Transfer* **2024**, *222*, 125209.
[59] J. Peoples, X. Li, Y. Lv, J. Qiu, Z. Huang, X. Ruan, *Int. J. Heat Mass Transfer* **2019**, *131*, 487.